



Research paper

Measuring affinity constants of 1450 monoclonal antibodies to peptide targets with a microarray-based label-free assay platform



J.P. Landry^a, Yaohuang Ke^b, Guo-Liang Yu^b, X.D. Zhu^{a,*}

^a Department of Physics, University of California, Davis, CA, 95616, USA

^b Epitomics, Inc, Burlingame, CA 94010, USA

ARTICLE INFO

Article history:

Received 15 October 2014

Received in revised form 11 December 2014

Accepted 12 December 2014

Available online 20 December 2014

Keywords:

Monoclonal antibody

Peptide

Affinity constants

Label-free detection

Microarray

Oblique-incidence reflectivity difference

ABSTRACT

Monoclonal antibodies (mAbs) are major reagents for research and clinical diagnosis. For their inherently high specificities to intended antigen targets and thus low toxicity in general, they are pursued as one of the major classes of new drugs. Yet binding properties of most monoclonal antibodies are not well characterized in terms of affinity constants and how they vary with presentations and/or conformational isomers of antigens, buffer compositions, and temperature. We here report a microarray-based label-free assay platform for high-throughput measurements of monoclonal antibody affinity constants to antigens immobilized on solid surfaces. Using this platform we measured affinity constants of over 1410 rabbit monoclonal antibodies and 46 mouse monoclonal antibodies to peptide targets that are immobilized through a terminal cysteine residue to a glass surface. The experimentally measured affinity constants vary from 10 pM to 200 pM with the median value at 66 pM. We compare the results obtained from the microarray-based platform with those from a benchmarking surface-plasmon-resonance-based (SPR) sensor (Biacore 3000).

© 2014 Elsevier B.V. All rights reserved.

1. Introduction

Highly adaptive structures in paratope regions of antibodies afford their specific recognition capabilities and thus enable them the primary defense against foreign pathogens in a living organism. This remarkable molecular attribute also makes antibodies the leading choice of reagents for diagnosis and extraction of biomarkers from samples in clinical laboratories and in laboratories of life/medical sciences. In recent years, monoclonal antibodies are actively and in some cases successfully explored as one of the major forms of biologic drugs, for inherently high target-specificity and in turn low required dosage to achieve same therapeutic efficacy (Beck et al., 2010; Nguyen et al., 2007; Weiner et al., 2010). Recent Ebola outbreaks in Africa and other parts of the world and the remarkable

promise of combinations of monoclonal antibodies as an effective cure of infected patients highlight the importance of and urgent need for antibody-based drugs and antibody research in general (Qiu et al., 2014; Weingartl et al., 2012).

Despite the aforementioned, most monoclonal antibodies from commercial vendors and in academic laboratories are not well characterized, in terms of quantitative binding properties against specific and non-specific targets. It is a common and often costly experience that one finds monoclonal antibodies against same antigen target but from different vendors or from the same vendor but of different lots to yield significantly different outcomes in “identically” executed assays. There are extensive studies revealing that on average 50% of commercial antibodies do not produce expected binding results as advertised and the success rate varies from 0% to 100% for different vendors (Perkel, 2013). Even from the same lot, qualitative outcomes of antibody-antigen binding assays may vary from one type of assay to

* Corresponding author.

E-mail address: xdzhu@physics.ucdavis.edu (X.D. Zhu).

another; and from one laboratory to another. Some variations originate from changes in the paratope of the antibody that are often inadequately characterized. Others have to do with assay conditions, protocol details, and conformational presentations (denatured vs. natural form, free form vs. constrained form as a conjugate to a large carrier or as an integral part of a large protein) of antigen targets that can be understood and anticipated only if kinetic and thermodynamic information on antibody-antigen binding reactions are known even in limited circumstances, instead of merely IHC and Western Blot data or even less. The main reason that most antibodies are so insufficiently characterized and validated is the cost, in terms of materials, instrumentation, and skilled labor. There clearly is a need for cost-effective assay platforms that yield high-quality kinetic and thermodynamic parameters on antibody-antigen binding reactions and on how outcomes of the reactions may vary from assay to assay as protocols and conformational constraints on antigens change.

We report a microarray-based label-free assay platform that affords high-throughput cost-effective measurement of binding curves of antibodies to antigen targets (Fei et al., 2013, 2008; Landry et al., 2012; Zhu et al., 2007). We applied this platform to determine binding constants of 1410 rabbit monoclonal antibodies and 46 mouse monoclonal antibodies to synthetic peptide targets that are immobilized through a terminal cysteine residue on a functionalized glass slide surface. The results compare well with measurements using a benchmark (but low throughput) SPR-based label-free sensor (Biacore 3000). Furthermore we find that the measured binding constants do not change when the target density changes by more than a factor of 4 (comparable to the target density in the SPR measurement) so that the average target separation is twice the dimension of a captured antibody, indicating that the measured binding constants are affinity constants instead of avidity constants that would involve both paratopes of bivalent antibody molecules.

2. Methods and materials

The essence of the present assay platform is as follows. Antigen targets are immobilized on a functionalized glass slide in form of a microarray in such a way that epitopes on the targets are available to subsequent solution-phase antibodies. The antigen microarray is incubated in solutions of specific antibodies raised against the targets at a series of concentrations. Afterward the microarray is kept in a constant flow of the buffer to allow antibody-antigen complexes formed during incubation to dissociate. Surface mass densities of antibody-antigen complexes on the microarray during incubation and subsequent dissociation are recorded in real time with a scanning ellipsometry sensor (Landry et al., 2012). The sensor measures the phase change of an illuminating optical beam as a result of antibody-antigen complex formation. The phase change has been shown proportional to the surface mass density of antibody-antigen complexes. The optical data yield binding curves that are subsequently used to extract binding kinetic constants (Landry et al., 2012).

2.1. Peptide antigen microarray

1456 antigens are synthetic peptides (15-aa with average molecular weight of 2 kDa) supplied by Eptomics, Inc (Burlingame, CA). They originate from a large collection of source proteins (See Supplemental Information) that are mostly targeted in drug discovery. At either N- or C-terminus, a cysteine residue is added intentionally. The peptides are lyophilized as received. To make printing solutions, each peptide is dissolved in 2 μ L DMSO and diluted further in 38 μ L 1 \times PBS to a final concentration of 0.25 mg/mL (~125 μ M). The solutions are deposited in a 384-well plate for microarray fabrication. Peptide microarrays are printed on epoxy-functionalized glass slides (ArrayIt, Sunnyvale, CA) using an OmniGrid 100 contact-printing robot (Digilab, Holliston, MA) with 100 μ m diameter stainless steel pins (Majer Precision Engineering, Tempe, AZ). Primary amine residues and thiol residues on the peptides react covalently with epoxide groups on the glass surface and anchor the peptides. A significant fraction of the peptides is immobilized through the terminal cysteine, making functional regions of these immobilized peptides intact and available in subsequent binding assays.

As shown in Fig. 1, on one functionalized glass slide, we print 6 identical peptide microarrays so that after assembled in a fluidic cartridge each microarray is housed in a separate reaction chamber (12 mm L \times 6 mm W \times 0.4 mm D). In the present study, each peptide microarray (Fig. 2(a)) consists of 4 identical subarrays as replicates, each having 100 distinct peptides and 20 control features in form of 8 rows \times 15 columns. The left-most and the right-most columns consist of bovine serum albumin (BSA) and one blank. 100 peptides, 3 BSA and 1 blank form the remaining 13 columns (Fig. 2(b)). The diameters of printed peptide spots vary from 80 μ m to 160 μ m due to variations in wetting property of the peptide solutions. For the present study, 1456 peptides are printed on 16 slides. We use 4 out of 6 microarrays on a glass slide to acquire a set of binding curves. The remaining two microarrays are for back-up. Before binding curve measurements, the peptide microarray is washed and blocked with a solution of BSA at 2 mg/mL in 1 \times PBS for 30 minutes and then washed and maintained in 1 \times PBS (Fei et al., 2008).

2.2. Monoclonal antibodies (MAbs)

To produce monoclonal antibodies, these peptides are conjugated to carrier protein KLH through the terminal cysteine residue using the standard maleimide conjugation scheme and Sulfo-SMCC cross-linkers (for example, see <http://www.piercenet.com/product/maleimide-activated-klh-kit>.) The conjugates are then introduced into rabbit or mouse for production of monoclonal antibodies. Harvested monoclonal antibodies are screened using direct peptide coating ELISA and western blot at Eptomics, Inc (Burlingame, CA) for specific binding. For direct peptide coating ELISA, we coated the ELISA plates using same peptides with terminal cysteine residues, either directly or having the peptides first conjugated to BSA and then using BSA-conjugated peptides for coating. We then added rabbit hybridoma supernatants to the plates and the binding of rabbit antibodies to the peptides were detected by HRP conjugated goat anti-rabbit secondary antibody (Jackson ImmunoResearch). 1410 rabbit mAbs and 46 mouse mAbs were

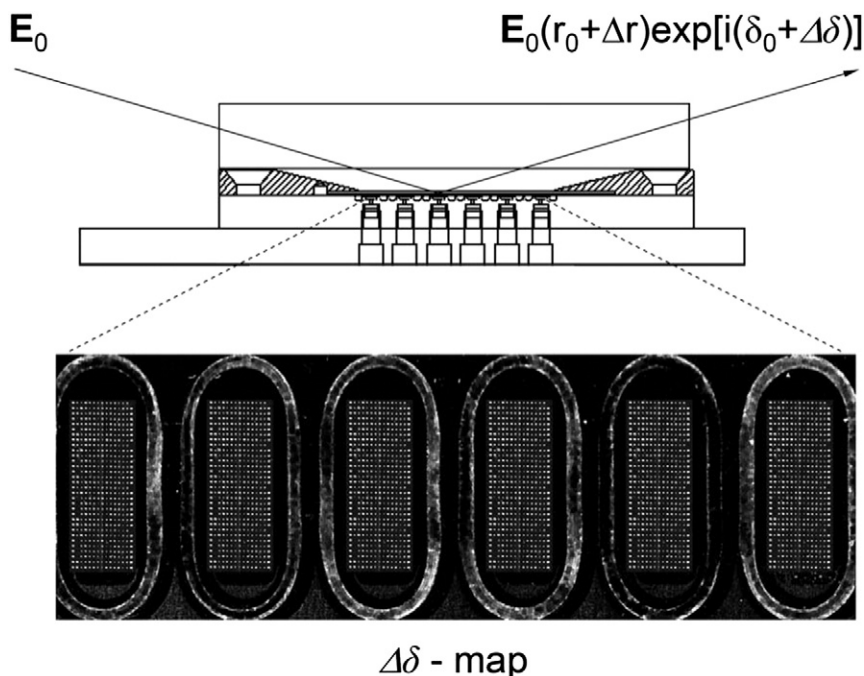


Fig. 1. Sketch of a microarray-based label-free assay platform, consisting of a 1" × 3" glass slide printed with 6 peptide target microarrays (the slide being an integral part of a 6-chamber fluidic assembly) and a scanning ellipsometry microscope (a.k.a. oblique-incidence reflectivity difference or OI-RD microscope). The microscope detects surface mass densities of target microarrays *before*, *during* and *after* reactions with unlabeled probes by measuring the extra phase change $\Delta\delta$ in a reflected optical beam due to targets or target-probe complexes on the glass surface. An OI-RD image of 6 peptide microarrays is shown. Each microarray is composed of 4 subarrays (for data statistics), and each subarray consists of 100 distinct 15-aa peptides and 20 control features including blanks.

selected. The selected antibodies are further purified and concentrated from supernatants by Nvigen, Inc (Santa Clara, CA) following a high-yield antibody enrichment protocol involving protein A/G coated magnetic beads (http://www.nvigen.com/docs/MagVigen_proteinAG_nanoparticles.pdf). Purified antibodies were quantified at Epitomics using SpectraDrop Micro-Volume Microplate/SpectraMax Microplate Reader (Molecular Devices) as follows. The antibodies were diluted with PBS (1:10 dilution) and 5 ul of the diluted antibodies were loaded onto SpectraDrop Micro-Volume Microplate (Molecular Device). The same buffer without the antibodies was also loaded as blank. SpectraMax Microplate Reader was used to read absorbance at 280 nm and in turn concentrations of the purified antibodies.

2.3. Scanning ellipsometry for label-free microarray detection

In this study the label-free sensor for real-time microarray detection is a scanning optical microscope that detects oblique-incidence reflectivity difference (OI-RD) due to an antigen microarray on a glass surface (Fei et al., 2008; Landry et al., 2012). The optical signals are proportional to the surface mass density of antigen-antibody complexes. The OI-RD sensor does not require structured surfaces such as gold films or dielectric waveguides for detection and has a large "field of view" that easily expands from a few mm² to 100 cm². It is particularly suitable for detection of large microarrays on low-cost glass slides.

The arrangement of the scanning OI-RD microscope is shown in Fig. 1 (Fei et al., 2008; Landry et al., 2012). A scan lens focuses a polarization-modulated laser beam ($\lambda = 633$ nm) to a 20- μ m diameter spot on the back surface of a glass slide printed with antigen microarrays. The printed surface is in contact with either a buffer or an antibody solution. Images of a microarray are obtained by scanning the focused beam across the surface at 20 μ m step size along the y-axis and by moving the microarray along the x-axis at the same step size with an encoded translation stage. Image "contrast" is the polarization change of the optical beam upon reflection from the surface. The ratio of reflectivities for p- and s-polarized components of the optical beam is given by $r_p/r_s = \tan \psi \cdot \exp(i\delta)$. The scanning OI-RD microscope measures the change in δ , namely, $\Delta\delta$. $\Delta\delta$ varies linearly with the surface mass density Γ of antigen-antibody complexes as follows (Fei et al., 2008; Landry et al., 2012),

$$\Delta\delta \cong \frac{-4\pi\sqrt{\epsilon_s}\cos\theta}{(\epsilon_0 - \epsilon_s)(\cot^2\theta - \epsilon_s/\epsilon_0)} \cdot \frac{(\epsilon_d - \epsilon_0)(\epsilon_d - \epsilon_s)}{\epsilon_d} \left(\frac{\Gamma}{\rho\lambda} \right). \quad (1)$$

ϵ_s , ϵ_0 , and ϵ_d are optical dielectric constants of the glass slide, the aqueous ambient, and the antigen-antibody complex layer, respectively. $\rho = 1.35$ g/cm³ is the volume mass density of globular proteins. θ is the incidence angle in the glass slide. Given $\epsilon_s = 2.31$, $\epsilon_0 = 1.77$, $\epsilon_d = 2.03$ and $\theta = 65^\circ$, a layer of antigen-antibody complexes with $\Gamma = 1$ ng/mm² yields $\Delta\delta = +6.4 \times 10^{-4}$. The current limit of our OI-RD

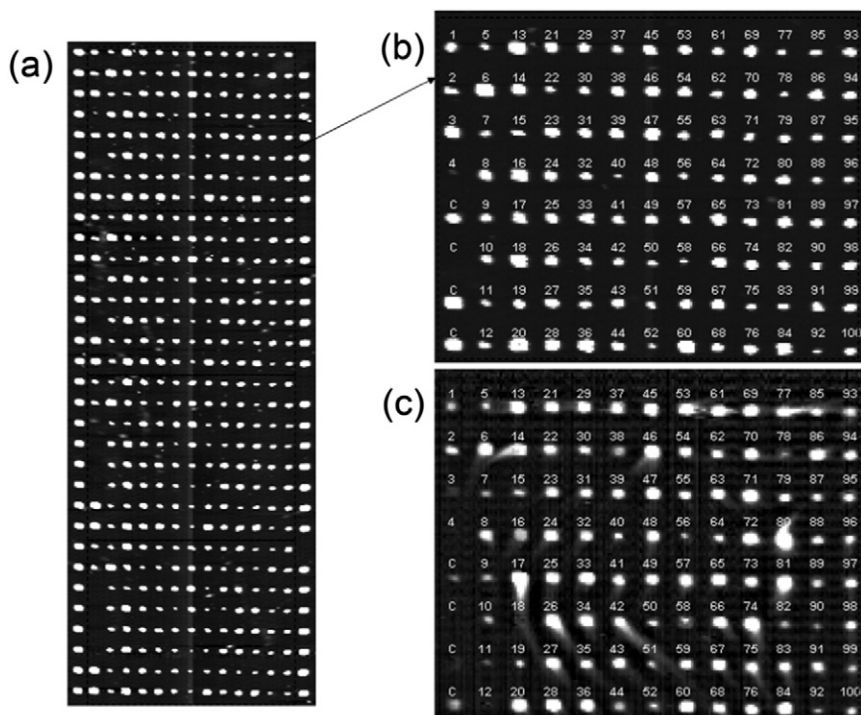


Fig. 2. (a) OI-RD image of one peptide microarray (with 4 subarrays from top to bottom) after printing and before further processing. The left and right edges of each subarray are bovine serum albumin (BSA) and a blank. Each pixel of the image is $20\ \mu\text{m} \times 20\ \mu\text{m}$. (b) OI-RD image of one subarray without the left-most and right-most edges. It consists of 100 15-aa peptides and 4 control features (3 BSA and 1 blank). The identities of the peptides are listed in Table 1. (c) Change in OI-RD image of the subarray after incubation with a monoclonal antibody mixture, at the individual probe concentration of 33 nM. The change measures the surface mass density of captured antibodies.

microscope is $|\Delta\delta| \sim 9 \times 10^{-6}$, corresponding to a surface mass density of $\sim 15\ \text{pg}/\text{mm}^2$.

2.4. High-throughput binding curve acquisition

To exploit the high-throughput capability of the microarray-based platform, we take advantage of the fact that each monoclonal antibody is raised and ELISA-selected specifically against one peptide target and the cross-reactivity can be neglected. As a result we incubate a peptide microarray of 100 immobilized targets in an equally concentrated mixture of 100 corresponding specific monoclonal antibodies. We make four mixtures with individual antibody concentration C at 100 nM, 33 nM, 11 nM, and 3.7 nM, respectively. Identical peptide microarrays in four reaction chambers are used to acquire binding curves at four antibody concentrations.

For binding curve measurement, we first flow $1 \times$ PBS through a reaction chamber at 0.01 mL/min for 30 min to acquire the baseline. We next replace $1 \times$ PBS with an antibody mixture at 5 mL/min in 5 s and then reduce the flow rate to 0.01 mL/min to allow the microarray to incubate in the mixture under the flow condition for 30 minutes (association phase of the reaction). Afterward, we replace the mixture with $1 \times$ PBS at 5 mL/min in 7 s and then reduce the flow rate to 0.01 mL/

min to allow antibody-antigen complexes to dissociate for 120 minutes (dissociation phase of the reaction).

To detect the amount of antigen-antibody complexes formed during association and dissociation phases of the reaction, we measure optical signals from a pixel in a target spot and two pixels in its neighboring unprinted region as the reference. The average of the signals read off the reference pixels is subtracted from the signal read off the target pixel to yield a background-corrected OI-RD signal $\Delta\delta$ (Landry et al., 2012). It takes 3 s for the scanning microscope to acquire one time-point from all 480 peptide targets in the microarray (120 targets in a subarray and 4 subarrays in one microarray). Each binding curve has 3600 time-points.

2.5. Langmuir binding model analysis

We use the 1-to-1 Langmuir reaction model and the global curve fitting to analyze the binding curves. During the association phase, the optical signal $\Delta\delta(t)$, proportional to the surface mass density of antibody-antigen complexes $\Gamma(t)$, is given by Landry et al., 2012

$$\Delta\delta(t) = \Delta\delta_0 \cdot \frac{k_{\text{on}} C}{k_{\text{on}} C + k_{\text{off}}} \left(1 - e^{-(k_{\text{on}} C + k_{\text{off}}) t} \right) \quad (2a)$$

Let t_0 be the time when the antibody mixture is replaced with $1 \times$ PBS to mark the start of the dissociation phase. During dissociation,

$$\Delta\delta(t) = \Delta\delta_0 \cdot \frac{k_{on}C}{k_{on}C + k_{off}} \left(1 - e^{-(k_{on}C + k_{off}) t_0}\right) e^{-k_{off}(t-t_0)} \quad (2b)$$

$\Delta\delta_0$ is proportional to the local peptide density where the target pixel is picked and thus varies from one replicate (in one subarray) to another (in another subarray) and from one binding curve (obtained in one chamber) to another (obtained in another chamber). As a result we fit the binding curve set for each antibody-antigen pair acquired at four antibody concentrations using k_{on} and k_{off} as global parameters valid for all four curves and $\Delta\delta_0$ as a local parameter adjustable for each curve. We compute the affinity constant (the equilibrium dissociation constant) as $K_d = k_{off}/k_{on}$ (Landry et al., 2012). In our present assay format, a set of four measurements in four chambers on one glass slide enable us to extract affinity constants for 100 antibody-antigen reactions.

2.6. Comparison with a benchmarking SPR-based label-free sensor

For comparison with a benchmark surface-plasmon-resonance (SPR) optical sensor for label-free binding curve acquisition (Loefas et al., 1991; Ritzefeld & Sewald, 2012), we performed binding curve measurements on 6 antibody-antigen pairs using Biacore 3000 (https://www.biacore.com/lifesciences/products/systems_overview/3000) under similar incubation conditions. C1 sensor chips originally functionalized with carboxylic acids are converted to being NHS-functionalized after incubation in a mixture of EDC and NHS for 10 min. An NHS-functionalized surface is electrophilic, similar to an epoxy-functionalized surface that we use to immobilize cysteine-terminated peptides. Both NHS and epoxide residues react strongly with nucleophilic residues such as amine and sulf-hydryl groups on cysteine-terminated peptides. As a result we do not expect significant differences in immobilization efficiency and presentation of cysteine-terminated peptides on these two surfaces, except for the final peptide surface density determined by that of NHS groups on a C1 sensor chip or epoxide groups on a commercial epoxy-functionalized glass slide. For target immobilization, we incubate amine-reactive sensor surfaces of Chamber 2, 3 and 4 on the CM1 chip in 45 μ M solutions of three different peptides for 20 min, according to the Biacore protocol. We then quench the surface of Chamber 1 and the unreacted surfaces of Chamber 2 through 4 by incubation in ethanolamine for 10 min followed by incubation in 0.2 mg/mL BSA for 10 min. Three rabbit monoclonal antibodies specifically raised against the 3 peptide targets in Chamber 2 through 4 are evenly mixed to make antibody mixtures at individual antibody concentration of $C = 135$ nM, 45 nM, and 15 nM. For binding reaction, a mixture flows through all four chambers on the C1 sensor chip simultaneously for same incubation times and at comparable flow rates as in the OI-RD/microarray-based experiments. The signal from Chamber 1 is used as the reference to remove the background in the signals from the other three chambers. Different C1 sensor chips are used for different antibody

mixtures as we do not regenerate the chip surface, - a procedure that is not reliable from our own experience.

3. Results and analysis

Fig. 2(a) displays the optical image in $\Delta\delta$ (OI-RD image) of one printed peptide microarray before further processing. It consists of 4 identical subarrays. Each subarray contains 100 peptide targets (Fig. 2(b)) and 20 control targets (bovine serum albumin and blank). The identities of these peptides (source proteins from which the peptides are derived) and their numeric assignments are listed in Table 1. Having 4 subarrays allows us to perform statistical analysis of binding kinetic parameters (Landry et al., 2012).

Fig. 2(c) shows the change in OI-RD image, obtained by subtracting the image taken before incubation from the image taken after incubation in an antibody mixture at the individual concentration of 33 nM. The contrast is proportional to the surface mass density of captured antibodies by immobilized peptide targets.

In Fig. 3(a) we display binding curves (from one replicate for clarity) of 100 monoclonal antibodies to respective peptide targets simultaneously acquired during incubation in the antibody mixture at individual probe concentration $C = 100$ nM (Landry et al., 2012). Fig. 3(b) combines binding curves acquired at 100 nM, 33 nM, 11 nM, and 3.7 nM into binding curve sets. Each set for one antibody-antigen pair is fit to Eqs. (2a) and (2b) with reaction rate constants k_{on} and k_{off} treated as global parameters (Landry et al., 2012). The results are listed in Table 1. The standard errors include contributions from the curve-fitting and variations from replicate to replicate in a microarray. For majority of the 100 antibody-peptide pairs, affinity constants K_d (equilibrium dissociation constants) are below 1 nM (10^{-9} M). The detection limit of K_d in the present study is 1 pM (10^{-12} M).

This procedure is repeated for the remaining 1356 monoclonal antibodies. The binding curve sets are fit to Eqs. (2a) and (2b) to yield association rates, dissociation rates, and affinity constants. These kinetic constants (k_{on} , k_{off} , and K_d) for all 1456 monoclonal antibodies against their respective peptide targets are list in Table S1 in Supplemental Information. To examine whether the binding kinetic constants are indeed affinity constants (monovalent) instead of avidity constant (bivalent) as each full rabbit antibody has two paratopes (two Fab domains), we repeated the association-dissociation curve measurement for three rabbit monoclonal antibodies with immobilized peptide targets at reduced surface densities (by reducing printing concentrations) so that the mean separation of the immobilized targets is twice the size of an IgG molecule. Though the captured rabbit antibody molecules per unit area are reduced in number by a factor of 4, the equilibrium dissociation constants K_d remain unchanged within a factor of 5. This shows that the measured K_d in the present study are indeed affinity constants.

To find the overall characteristic of affinity constants of all 1410 rabbit monoclonal antibodies and the performance of our present OI-RD/microarray-based assay platform, we show in Fig. 4 a plot of dissociate rate constants k_{off} as a function of dissociation rate constants k_{on} . Each point corresponds to one antibody-antigen pair and the ratio of

Table 1

Numeric ID and source proteins of 100 peptides along with association rates k_{on} , dissociation rates k_{off} , and equilibrium dissociation constants $K_d = k_{off} / k_{on}$ with specific monoclonal antibodies. Peptide#4 yielded no binding curve data.

| Peptide ID | Original proteins from which peptides are derived | k_{on} $10^5 s^{-1} M^{-1}$ | k_{off} $10^{-5} s^{-1}$ | K_d μM |
|------------|---|----------------------------------|-------------------------------|------------------|
| 1 | EEA1 | 2.3 | 2.8 | 120 |
| 2 | CD3 epsilon | 2.0 | 1.3 | 64 |
| 3 | MCSF | 18.0 | 3.2 | 18 |
| 4 | MLH1 | – | – | – |
| 5 | M110614 (1–6) | 1.0 | 1.3 | 129 |
| 6 | PK071 (22–20) | 0.7 | 10.1 | 1370 |
| 7 | Histone H3 (tri methyl K27) - ChIP Grade | 7.5 | 4.6 | 61 |
| 8 | Histone H3 - ChIP Grade | 3.2 | 6.1 | 190 |
| 9 | Aurora B | 9.6 | 2.5 | 27 |
| 10 | Histone H3 (phospho S10) - ChIP Grade | 12.8 | 3.9 | 31 |
| 11 | APOBEC3G | 21.3 | 6.1 | 29 |
| 12 | HP1 alpha - Heterochromatin marker | 2.8 | 20.9 | 750 |
| 13 | PK036 (E7-B7) | 0.0 | 2.4 | 4960 |
| 14 | PK011 (48-89) | 0.0 | 1.9 | 5400 |
| 15 | PK022 (19-76) | 5.3 | 1.8 | 33 |
| 16 | PK040 (D0-G11) | 2.2 | 4.9 | 227 |
| 17 | PK023 (D11-7) | 1.0 | 1.2 | 118 |
| 18 | PK066 (20-119) | 4.8 | 4.9 | 103 |
| 19 | M120404 (A2-F6) | 9.9 | 1.5 | 15 |
| 20 | M120505-1 (1-B11) | 9.5 | 2.9 | 31 |
| 21 | DLGAP4 | 3.2 | 0.2 | 5.3 |
| 22 | Kallikrein 5 | 4.1 | 0.2 | 5.4 |
| 23 | PPP2CB | 2.4 | 2.2 | 92 |
| 24 | GLA | 3.8 | 0.9 | 24 |
| 25 | ACAT1 | 2.4 | 0.0 | 1.1 |
| 26 | Septin-10 | 1.8 | 0.3 | 15 |
| 27 | DOK5 | 4.0 | 4.2 | 106 |
| 28 | WDR5 | 4.2 | 0.6 | 15 |
| 29 | Lumican | 2.8 | 0.4 | 16 |
| 30 | NEDD4L Phospho (pS448) | 3.1 | 0.4 | 12 |
| 31 | Growth Arrest Specific Protein 7 | 3.3 | 0.9 | 26 |
| 32 | PPP2CB | 1.7 | 0.1 | 7.6 |
| 33 | Glutamate dehydrogenase 1 | 1.7 | 1.5 | 91 |
| 34 | CDK5RAP3 | 2.0 | 0.3 | 15 |
| 35 | CLPX | 2.4 | 2.1 | 86 |
| 36 | Fbx32 | 2.6 | 0.6 | 22 |
| 37 | Pyruvate Dehydrogenase E1-alpha | 2.1 | 0.6 | 30 |
| 38 | NR5A1 | 0.2 | 2.8 | 1730 |
| 39 | Na + /K + ATPase a2 | 3.5 | 1.9 | 55 |
| 40 | BXDC1 | 0.7 | 1.8 | 235 |
| 41 | U1A | 1.6 | 0.8 | 48 |
| 42 | TCP1 eta | 2.8 | 0.4 | 13 |
| 43 | TAF1 | 2.4 | 0.3 | 13 |
| 44 | VMAT1 | 0.4 | 0.9 | 204 |
| 45 | COG7 | 1.8 | 0.7 | 41 |
| 46 | Glypican 4 | 1.5 | 0.1 | 7.4 |
| 47 | DNAJA2 | 0.8 | 0.6 | 78 |
| 48 | HoxC13 | 2.6 | 4.7 | 178 |
| 49 | PARM-1 | 1.8 | 0.2 | 10 |
| 50 | Alpha-1B Adrenergic Receptor | 8.1 | 0.6 | 7.7 |
| 51 | hnRNP E1 | 1.7 | 3.6 | 208 |
| 52 | hnRNP E1 | 2.3 | 0.5 | 20 |
| 53 | SHIP2 | 3.3 | 0.0 | 1.5 |
| 54 | CHMP1a | 2.4 | 1.1 | 48 |
| 55 | BASP1 | 1.8 | 2.0 | 109 |
| 56 | CUL2 | 1.7 | 1.2 | 70 |
| 57 | REEP5 | 1.2 | 0.5 | 41 |
| 58 | MRPS31 | 1.6 | 1.0 | 60 |
| 59 | H-Cadherin | 2.0 | 1.2 | 63 |
| 60 | Ribosomal Protein S15 | 1.1 | 0.2 | 20 |
| 61 | TTC14 | 4.6 | 0.3 | 7.1 |
| 62 | Histone Deacetylase 11 | 2.9 | 1.9 | 65 |
| 63 | TPMT | 1.9 | 1.8 | 93 |
| 64 | PSAP | 5.2 | 4.8 | 92 |
| 65 | DDX20 | 1.6 | 1.2 | 74 |
| 66 | CDH29 | 1.6 | 0.2 | 13 |

(continued on next page)

Table 1 (continued)

| Peptide ID | Original proteins from which peptides are derived | k_{on} | k_{off} | K_d |
|------------|---|----------------------|------------------|---------|
| | | $10^5 s^{-1} M^{-1}$ | $10^{-5} s^{-1}$ | μM |
| 67 | AARS | 2.0 | 0.2 | 12 |
| 68 | TXNRD1 | 1.8 | 0.1 | 6.6 |
| 69 | C1D | 2.1 | 0.2 | 11 |
| 70 | PRSS2 | 3.5 | 0.0 | 1.1 |
| 71 | TMEM45A | 1.8 | 0.0 | 1.2 |
| 72 | AKR1C1 | 2.3 | 0.0 | 0.88 |
| 73 | AK2 | 2.8 | 1.4 | 50 |
| 74 | CDCA3 | 3.0 | 0.2 | 6.5 |
| 75 | EDG2 | 5.1 | 0.7 | 13 |
| 76 | Beta-Glucuronidase | 2.7 | 1.2 | 46 |
| 77 | DEK | 1.0 | 0.3 | 24 |
| 78 | GPI | 1.7 | 0.9 | 55 |
| 79 | SPSB2 | 2.1 | 1.4 | 67 |
| 80 | PSMG1 | 1.4 | 0.0 | 1.1 |
| 81 | SPESP1 | 2.7 | 0.8 | 28 |
| 82 | IRF-6 | 2.0 | 5.7 | 283 |
| 83 | Doublecortin | 2.5 | 1.6 | 61 |
| 84 | POGZ | 4.9 | 0.6 | 12 |
| 85 | UGP2 | 3.3 | 1.6 | 49 |
| 86 | ACOT7 | 2.3 | 0.3 | 15 |
| 87 | ZAK | 9.2 | 4.2 | 45 |
| 88 | ACP1 | 6.4 | 1.7 | 26 |
| 89 | Glutamate dehydrogenase 1/2 | 20.6 | 5.1 | 25 |
| 90 | Napsin A | 3.7 | 1.8 | 48 |
| 91 | ERH | 2.0 | 4.7 | 239 |
| 92 | STOM | 4.4 | 1.9 | 43 |
| 93 | ISG20 | 1.8 | 4.4 | 242 |
| 94 | eIF-2A | 3.7 | 1.8 | 49 |
| 95 | HBXIP | 2.8 | 0.8 | 28 |
| 96 | Cathepsin L2 | 2.7 | 3.5 | 131 |
| 97 | UGT1A | 2.6 | 0.3 | 10 |
| 98 | Galectin-10 | 1.2 | 0.9 | 71 |
| 99 | ENO3 | 3.4 | 4.9 | 144 |
| 100 | TST | 2.0 | 1.5 | 78 |

the two constants is the affinity constant K_d for the pair. Contours of constant K_d are oblique straight lines shown so that the distribution of K_d can be seen along these lines. Histograms of the two kinetic constants and K_d are also displayed in the figure. Except for a small peak near $10^{-7} s^{-1}$ (the limit of the present study), k_{off} are centered at around $10^{-5} s^{-1}$ with a full-width-at-half-max (FWHM) spanning one order of magnitude. k_{on} are centered at around $10^5 s^{-1} M^{-1}$ with a FWHM also over one order of magnitude. This makes K_d for 1410 rabbit monoclonal antibody-peptide pairs to range from 20 pM to 200 pM with a median of 66 pM. For the 46 monoclonal mouse antibodies, albeit a much smaller collection, we find K_d to their respective peptide antigens ranging from 30 pM to 300 pM with a median of 72 pM, close to the median for 1410 rabbit monoclonal antibodies.

Surface-plasmon-resonance-based (SPR) sensors such as Biacore 3000 were the first commercial label-free platform for biomolecular binding curve assays (Loefas et al., 1991). Although all optical-reflection-based sensors including SPR sensors measure same surface mass density changes on solid surface, subsequent label-free sensors are often required to benchmark against an SPR sensor (Zhu, 2006). For this purpose, we separately measured binding curves of 6 rabbit monoclonal antibodies against their peptide targets using both the OI-RD platform and a Biacore 3000.

Fig. 5 shows binding curve sets of 3 rabbit monoclonal antibodies to peptide antigens obtained with the OI-RD platform and a Biacore 3000 under same reaction conditions except for immobilized target density and flow channel depth. The peptide targets are derived from *EGFR Phospho (pY1068)*, *CD34*, and *Cytokeratin 15*. The quality of binding curves is comparable. It is noteworthy that net surface mass density changes in the SPR measurements are a factor of 4 smaller than those found in the OI-RD/microarray-based measurements, indicating that peptide target densities on the gold-coated surface of a C1 sensor chip (following the Biacore 3000 protocol) are smaller by at least a factor of 4 than the target densities achieved on the epoxy-coated glass surface. It means that the mean separation between the immobilized peptide on the gold-coated surface is at least twice the size of an IgG molecule and the binding curves obtained with Biacore 3000 should yield affinity constants instead of avidity constants. We fit binding curve sets to Eqs. (2a) and (2b) with k_{on} and k_{off} as global parameters. The results are listed in Table 2. K_d 's measured using both label-free sensors are comparable within a factor of 4. This once again confirms that our OI-RD/microarray-based assay platform truly measures affinity constants of antibodies against peptide antigens.

A closer examination of binding curves and fits to the 1-to-1 Langmuir reaction model (i.e., Eqs. (2a) and (2b)) reveals that there are more than one presentation of a

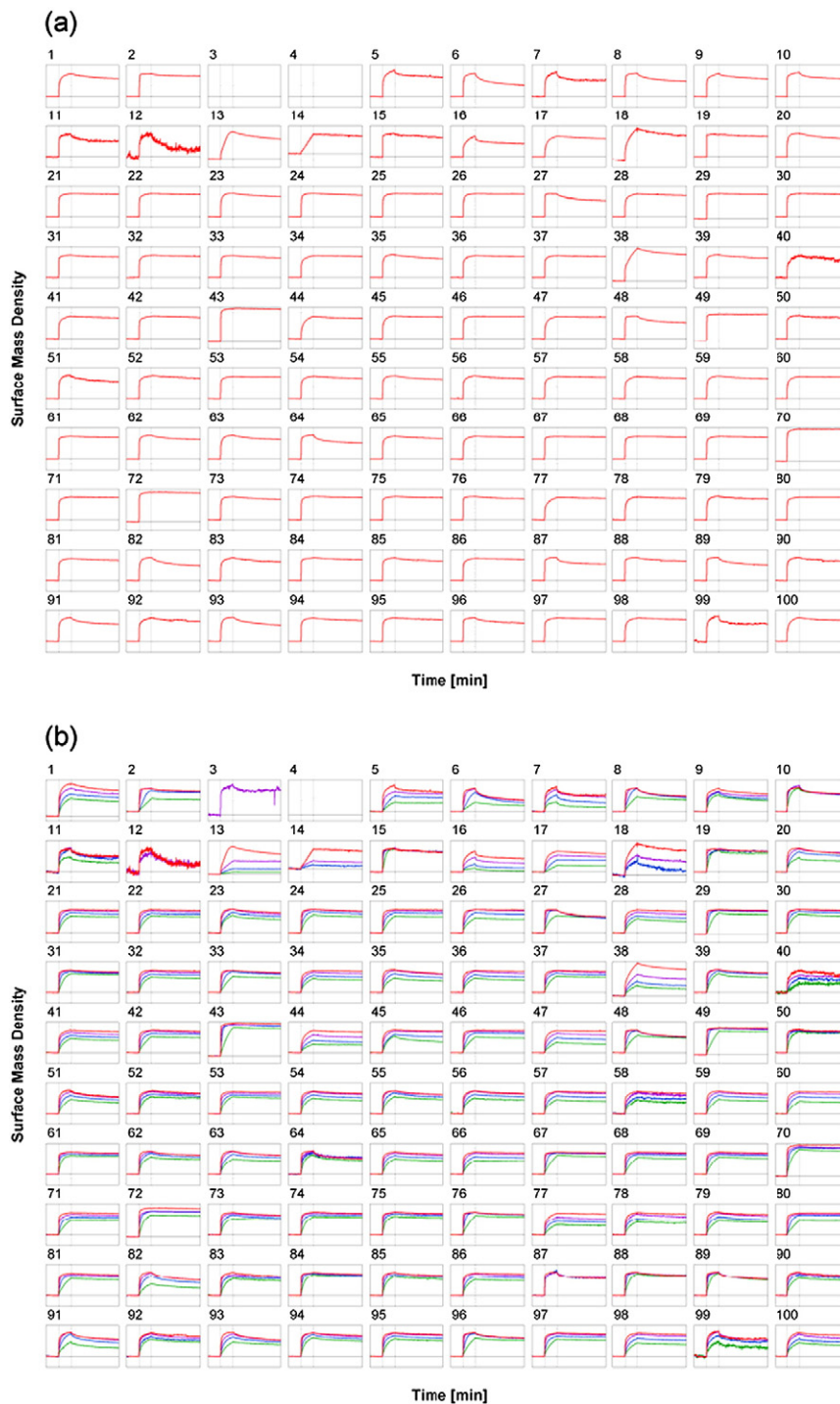


Fig. 3. (a) Binding curves of 100 monoclonal antibodies to respective peptide antigen targets *simultaneously acquired during incubation* in the antibody mixture with individual probe concentration at $C = 100$ nM. The vertical axis is the surface mass density change that has a full scale of 10 ng/mm^2 . The measurement on peptide#4 did not yield binding curves. (b) Binding curve sets for the same 100 antibodies acquired in 4 separate chambers at individual probe concentrations of 100 nM, 33 nM, 11 nM, and 3.7 nM. The curve sets are fit to the 1-to-1 Langmuir reaction model with k_{on} and k_{off} as global parameters. The equilibrium dissociation constant for each antibody-antigen pair is computed as $K_d = k_{off}/k_{on}$. These parameters are listed in Table 1.

peptide target upon immobilization so that the specific antibody molecules in the solution form more than one type of complexes with the immobilized peptides, each

characterized with a distinct affinity constant (Landry et al., 2012; Sun et al., 2008). This is particularly obvious for binding curves obtained with the Biacore 3000. More

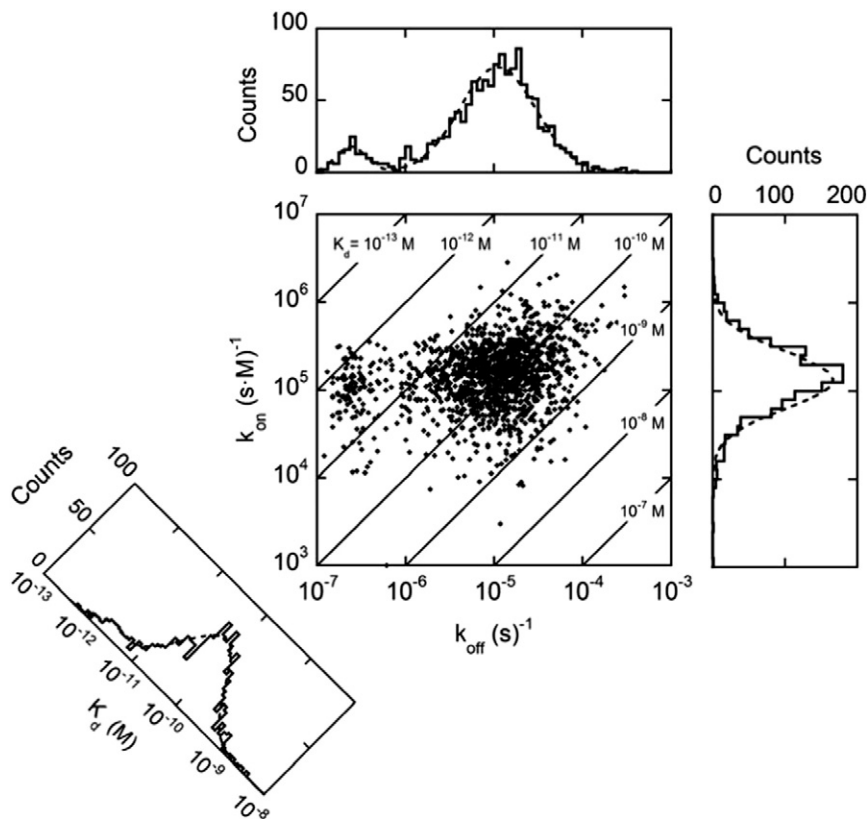


Fig. 4. Maps of association rates, dissociation rates, and equilibrium dissociation constants for 1410 rabbit monoclonal antibodies with specific 15-aa peptide antigen targets, from binding curves obtained using the microarray-based label-free assay platform. Each point is from one antibody-peptide pair. Diagonal lines show contours of constant equilibrium dissociation constant $K_d = k_{\text{off}} / k_{\text{on}}$ in unit of molar (M).

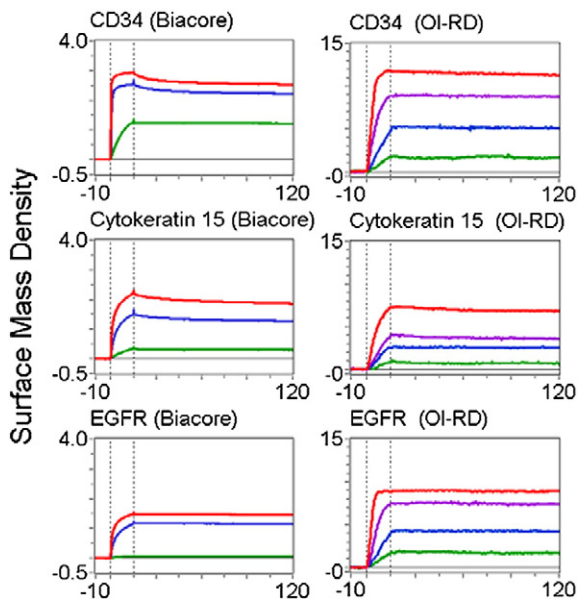


Fig. 5. Binding curve sets of 3 rabbit monoclonal antibodies with peptide targets, from *CD34*, *Cytokeratin 15*, and *EGFR* respectively, obtained using both Biacore 3000 and the microarray-based platform for comparison. The curve sets were globally fit to yield equilibrium dissociation constants (K_d). The results are listed in Table 2.

weakly bound complexes have significantly shorter dissociation times and may not be detected by endpoint measurements such as most fluorescence-based assays where measurements are performed after washing. When the assay time (incubation plus dissociation phase) is short, the presence of more weakly bound complexes makes “apparent” affinity constants determined from the fit to the 1-to-1 Langmuir reaction model larger than the constants for more tightly bound complexes. The latter are more closely resemble the complexes formed in solution.

4. Discussion and conclusion

This study is the first where specific affinity constants of over 1400 monoclonal antibodies raised with the same technology against synthetic peptide targets are determined on a microarray-based label-free assay platform. Qualities of binding curves and affinity constants obtained from this platform are comparable to those of a benchmark SPR-based platform (Biacore 3000).

4.1. Affinity constants for rabbit monoclonal antibodies to specific targets

Because 1410 peptide targets come from a wide range of proteins or protein fragments, Fig. 4 represents the typical

Table 2

Comparison of the OI-RD/microarray-based assay platform with Biacore 3000 in characterization of specific affinity constants and rate constants of monoclonal rabbit antibodies with 6 immobilized peptide targets.

| Original proteins from which 6 peptides are derived | Biacore 3000 | | | OI-RD scanning sensor | | |
|---|--------------------------------------|--------------------------|-------|--------------------------------------|--------------------------|-------|
| | k_{on} | k_{off} | K_d | k_{on} | k_{off} | K_d |
| | $10^5 \text{ s}^{-1} \text{ M}^{-1}$ | 10^{-5} s^{-1} | pM | $10^5 \text{ s}^{-1} \text{ M}^{-1}$ | 10^{-5} s^{-1} | pM |
| CD34 | 3.5 | 1.4 | 41 | 0.37 | 0.43 | 115 |
| Cytokeratin 15 | 7.3 | 1.8 | 247 | 0.16 | 0.89 | 564 |
| EGFR Phospho | 0.69 | 0.058 | 8.5 | 0.42 | 0.08 | 19 |
| Glucagon | 3.7 | 2.6 | 70 | 0.35 | 1.2 | 331 |
| Glut-1 | 4.6 | 1.1 | 24 | 0.36 | 0.028 | 7.7 |
| Vimentin | 2.3 | 7.1 | 306 | 0.25 | 4.3 | 1700 |

distribution of affinity constants (20 ~ 200 pM) for rabbit monoclonal antibodies raised with a hybridoma technology of Epitomics, Inc against 15-aa peptides, measured using solid-surface-based assays. A small fraction of the 1410 rabbit monoclonal antibodies have affinity constants in the order of 1 ~ 2 pM with dissociation rates close to $k_{off} = 10^{-7} \text{ s}^{-1}$ (the limit of the present study). We should note here that by immobilizing peptide targets on a solid surface, available conformational isomers for such a peptide are significantly reduced in number from those for a same but free peptide in a solution so that association rates k_{on} of corresponding antibodies to *immobilized* peptides are generally larger. Consequently affinity constants obtained from solid-surface-supported binding curve assays including the present OI-RD/microarray-based assays and the SPR-based assays are expected to be smaller than the affinity constants obtained when both the antibody and the peptide antigen are in solution. A more detailed study of this topic will be separately reported.

4.2. Affinity constants of mouse monoclonal antibodies vs. affinity constants of rabbit monoclonal antibodies

For a pool of 46 monoclonal antibodies, their affinity constants to peptide targets cover a similar range (30 pM ~ 300 pM) as that for 1410 rabbit monoclonal antibodies (20 ~ 200 pM). Within the limit of detection and the scope of this study (i.e., the pool size of investigated mouse monoclonal antibodies), it is inconclusive whether rabbit monoclonal antibodies have much higher affinity than mouse monoclonal antibodies.

4.3. Performance characteristics of the OI-RD/microarray-based assay platform

Using the OI-RD/microarray assay platform, we have measured K_d of protein-ligand binding reactions over a range from mM to 1 pM. Fig. 4 highlights some of performance features of the platform such as limits of detectable kinetic constants and the extent of the mass transport effect on association rate measurement. The lower bound of detectable dissociation rates k_{off} is 10^{-7} s^{-1} . It is determined by the duration of the dissociation phase and the overall noise level of the assay platform (Landry et al., 2012). It may be further reduced by another order of magnitude with the improvement of the noise reduction. Though increasing the dissociation phase duration seems an equal option as well, it is often not practical. The upper bound of k_{off} and k_{on} C is the larger of the sampling rate (0.33 s^{-1} in the present study) and the rate

set by the effect of mass transport. As shown Fig. 4 this platform yields k_{on} as large as $10^6 \text{ M}^{-1} \text{ s}^{-1}$ at antibody probe concentrations as high as 100 nM, thus the upper bound for k_{on} C and k_{off} for the present platform is mostly determined by the sampling rate of 0.33 s^{-1} . It is worth emphasizing that key characteristics of antibody-antigen binding reaction or antibody-antigen complexes are dissociation rate constants k_{off} . Since the latter are usually small for typical antibody-antigen pairs, their measurements over a long dissociation phase are not subject to the mass transport effect.

Binding curves in Fig. 3 exhibit the sensitivity of the microarray-based platform for antibody characterization. A full layer of antibody molecules has a surface mass density of 5 ~ 16 ng/mm², depending upon the average orientation of the aspheric molecules. It is a factor of 1000 larger than the background noise (15 pg/mm²) in our present assay system. Though it is not yet as sensitive as a Biacore 3000 (~1 pg/mm²), it is more than sufficient for assaying antibody-antigen binding reaction. Low cost per binding curve set and high-throughput make the microarray-based assay platform advantageous over Biacore 3000 or other similar platforms. As reported by Fei and coworkers (Fei et al., 2013), this platform has the capability to measure the temperature dependence of affinity constants and thus thermodynamic parameters of binding reactions that reveal details of antibody-antigen complex formation, such as entropic contributions to the stability of the complexes from available antigen isomers and effects of solvation/de-solvation.

4.4. Application of binding kinetic constants to understanding of various endpoint assays

Kinetic constants of antibody-antigen binding reactions including k_{on} and k_{off} as well as K_d obtained from microarray-based measurements can be qualitatively and even quantitatively applied to understanding of antibody binding to peptides/proteins in various endpoint assays such as ELISA; immunoblotting; immuno-precipitation; immuno-histochemistry, etc. under different conditions or protocols. For a specific antibody-antigen reaction to reach saturation in any of these endpoint assays the association rate constant k_{on} determines sufficient and but not excessive incubation times for a fixed antibody concentration or alternatively required antibody concentrations for a prescribed incubation time, while the dissociation rate constant determines the amount of the antibody-antigen complexes that survive repeated washing cycles. Furthermore dissociation rate constants for non-specific reactions of the same antibody with the backgrounds determine the effectiveness of

washing cycles as the product of the total washing time and the non-specific dissociation rate constant should be much larger than unity. Poor performances of antibodies in these assays can be analyzed and understood in terms of (1) whether adequate incubation times are allocated for formation of intended antibody-antigen complexes, (2) whether washing cycles are excessive so that most intended antibody-antigen complexes may not survive; (3) whether washing cycles are sufficient for unintended complexes formed by same antibodies and background epitopes to become dissociated and removed; (4) whether the buffer condition during incubation and/or washing cycles in a specific protocol have modified binding kinetic constants and in turn the endpoints of the assay.

In conclusion, we measured affinity constants of 1410 rabbit monoclonal antibodies and 46 mouse monoclonal antibodies to specific peptide targets on a microarray-based label-free binding curve assay platform. Affinity constants of rabbit monoclonal antibodies to immobilized peptide targets range from 20 to 200 pM with a median of 66 pM. The number of investigated mouse monoclonal antibodies is not large enough for such a general conclusion. We demonstrated that the ellipsometry/microarray-based assay platform is a high-throughput, cost-effective means of characterizing antibody affinity constants. In addition to the application as described in this study, this platform is useful for ranking/binning antibodies and evaluating cross-reactivity against a wide range of non-specific targets. Beyond antibodies, this platform is also suited for profiling a protein probe by affinity constants against a large collection of peptides that differ from each other by single amino-acids.

Supplementary data to this article can be found online at <http://dx.doi.org/10.1016/j.jim.2014.12.011>.

Acknowledgements

This work was supported by the University of California under U C Discovery Grant #bio09-156225 and in part by National Institutes of Health under R01-HD065122.

References

- Beck, A., Wurch, T., Bailly, C., Corvaia, N., 2010. Strategies and challenges for the next generation of therapeutic antibodies. *Nat. Rev. Immunol.* 10 (5), 345 (May).
- Fei, Y.Y., Landry, J.P., Sun, Y.S., et al., 2008. A novel high-throughput scanning microscope for label-free detection of protein and small-molecule chemical microarrays. *Rev. Sci. Instrum.* 79 (1), 013708 (Jan).
- Fei, Y.Y., Landry, J.P., Li, Y., et al., 2013. An optics-based variable-temperature assay system for characterizing thermodynamics of biomolecular reactions on solid support. *Rev. Sci. Instrum.* 84 (11), 114102 (Nov).
- Landry, J.P., Fei, Y.Y., Zhu, X.D., 2012. Simultaneous measurement of 10,000 protein-ligand affinity constants using microarray-based kinetic constant assays. *Assay Drug Dev. Technol.* 10, 250 (June).
- Loefas, S., Malmqvist, M., Roennberg, I., Stenberg, E., Liedberg, B., Lundstroem, I., 1991. Bioanalysis with surface plasmon resonance. *Sensors Actuators B* 5 (1–4), 6.
- Nguyen, M., Marcellus, R.C., Roulston, A., et al., 2007. Small molecule obatocax (GX15-070) antagonizes MCL-1 and overcomes MCL-1-mediated resistance to apoptosis. *Proc. Natl. Acad. Sci. U. S. A.* 104 (49), 19512 (Dec 4).
- Perkel, J.M., 2013. The antibody challenge. *Biotechniques* 56, 4.
- Qiu, X., Wong, G., Audet, J., et al., 2014. Reversion of advanced Ebola virus disease in nonhuman primates with ZMapp. *Nature* 514 (7520), 47 (Oct 2).
- Ritzfeld, M., Sewald, N., 2012. Real-time analysis of specific protein-DNA interactions with surface plasmon resonance. *J. Amino Acids* 2012, 19.
- Sun, Y.S., Landry, J.P., Fei, Y.Y., et al., 2008. Effect of fluorescently labeling protein probes on kinetics of protein-ligand reactions. *Langmuir* 24 (23), 13399 (Dec 2).
- Weiner, L.M., Surana, R., Wang, S., 2010. Monoclonal antibodies: versatile platforms for cancer immunotherapy. *Nat. Rev. Immunol.* 10 (5), 317 (May).
- Weingartl, H.M., Embury-Hyatt, C., Nfon, C., Leung, A., Smith, G., Kobinger, G., 2012. Transmission of Ebola virus from pigs to non-human primates. *Sci. Rep.* 2, 811.
- Zhu, X.D., 2006. Comparison of two optical techniques for label-free detection of biomolecular microarrays on solids. *Opt. Commun.* 259 (2), 751 (Mar 15).
- Zhu, X.D., Landry, J.P., Sun, Y.S., Gregg, J.P., Lam, K.S., Guo, X.W., 2007. Oblique-incidence reflectivity difference microscope for label-free high-throughput detection of biochemical reactions in a microarray format. *Appl. Opt.* 46 (10), 1890 (Apr 1).